

Topographic meandering of Antarctic Circumpolar Current and Antarctic Circumpolar Wave in the ice-ocean-atmosphere system

M. Nuncio,¹ Alvarinho J. Luis,¹ and X. Yuan²

Received 25 February 2011; revised 4 April 2011; accepted 4 April 2011; published 6 July 2011.

[1] Topographic meandering of Antarctic Circumpolar Current (ACC) is found to be an impediment in the propagation of Antarctic Circumpolar Wave (ACW) in the Indian Ocean sector of Antarctica. Reasons for this are attributed to the southward advection of the ACW anomalies associated with the topographic meandering of the ACC. The southward meandering of ACC facilitates warming up of the region east of 20°E by about 1°C during winter, thereby reducing the sea ice; these processes interfere with the eastward propagating positive sea-ice anomalies, and reduce its strength. Warming of ocean induced by topographic meandering leads to upward vertical velocities between 40°–60°E, where the ocean surface velocities are weak and southward, and the vertical/meridional advection of temperature dominates the zonal advection in the atmosphere. This results in the decoupling of the ACW in the region east of 40°E. In regions outside the Indian Ocean sector, vertical advection is minimum and zonal velocity of ACC becomes positive, which facilitates the ACW propagation in the Central Pacific, Ross and Weddell Seas. **Citation:** Nuncio, M., A. J. Luis, and X. Yuan (2011), Topographic meandering of Antarctic Circumpolar Current and Antarctic Circumpolar Wave in the ice-ocean-atmosphere system, *Geophys. Res. Lett.*, 38, L13708, doi:10.1029/2011GL046898.

1. Introduction

[2] Ever since its discovery, the Antarctic circumpolar wave (ACW) [White and Peterson, 1996] is one of the most studied climatic phenomena in the Southern Hemisphere. The ACW propagates eastward with the Antarctic Circumpolar Current (ACC) with a periodicity of 4–5 years and take approximately 8–10 years to encircle the globe. The presence of this circumpolar wave was detected in Atmospheric Temperature (AT), Sea Surface Temperature (SST), Sea-ice, Sea-level Pressure (SLP) and mean wind stress (MWS) [White and Peterson, 1996]. White et al. [1998] described the ACW as a self organisation within the global ocean-atmosphere system that requires the spherical shape of the rotating earth for its propagation and mean meridional temperature gradient for its maintenance. With multi-decadal scale intensification and weakening, the

ACW periodicity dominated the Dronning Maud Land ice core records of the last two millennia [Fischer et al., 2004]. Though the ACW was first discovered as a wave number-2 phenomenon (two highs and two lows along a latitude circle), higher wave numbers, wavenumber-3 and wavenumber-4 and frequencies were discovered with major contribution coming from a frequency of 4 cycles per year (cpy) [Jacobs and Mitchell, 1996]. The presence of more than one wave number was noted by other authors as well [Christoph et al., 1998; Cai et al., 1999; Comiso, 2000; Haarsma et al., 2000; Connolley, 2003; Venegas, 2003]. Using singular value decomposition, Venegas [2003] found that most of the ACW's variance comes from a linear combination of a propagating wave-3 pattern with a periodicity of 3 years and a propagating wave-2 pattern with a periodicity of 5 years, each having a distinct origin. Wave-3 is a result of the interaction between a spatially fixed atmospheric pattern and oceanic anomalies advected by the ACC, whereas wave-2 is generated in the western hemisphere by ENSO [Yuan, 2004]. There are many theories regarding the origin of ACW. The 4–5 year periodicity observed in the ACW links it with the ENSO [White and Peterson, 1996; Peterson and White, 1998; Cai and Baines, 2001; Park et al., 2004]. Qiu and Jin [1997] pointed out that the ACW is a result of coupled instability of the ACC and overlying atmosphere. The significance of ocean-atmosphere coupling was found in other model studies as well. The model ACW was sluggish without an atmospheric coupling to the ocean (10–14 years to encircle the globe) than the one involving ocean atmospheric coupling (8 years to encircle the globe) [White et al., 1998].

[3] A simple mechanism for the ACW propagation is as follows [Venegas, 2003]. The geostrophic balance between low and high pressure centres gives rise to poleward/equatorward flows, resulting in the surface atmosphere temperature anomalies, which in turn induces SST anomalies by direct warming/cooling as a result of reduced/enhanced heat fluxes. This process promotes sea-ice loss/gain. The warm/cool SST anomalies advected by the ACC weaken the high/low pressure eastward. Modeling and descriptive studies also underline the importance of ACC in advecting the SST anomalies eastwards [Cai et al., 1999; Peterson and White, 1998; White et al., 2002; White and Annis, 2004]. In a model study by White et al. [1998] maintenance of the model ACW is achieved through a balance between anomalous meridional Ekman heat advection and anomalous sensible-plus-latent heat loss to the atmosphere. Based on a linear theory for a circumpolar wave that involves the Sverdrup response of ocean and atmosphere to the mean meridional temperature gradient and vertical advection respectively, Talley [1999]

¹National Centre for Antarctic and Ocean Research, Vasco da Gama, India.

²Ocean and Climate Physics Laboratory, Lamont Doherty Earth Observatory, Palisades, New York, USA.

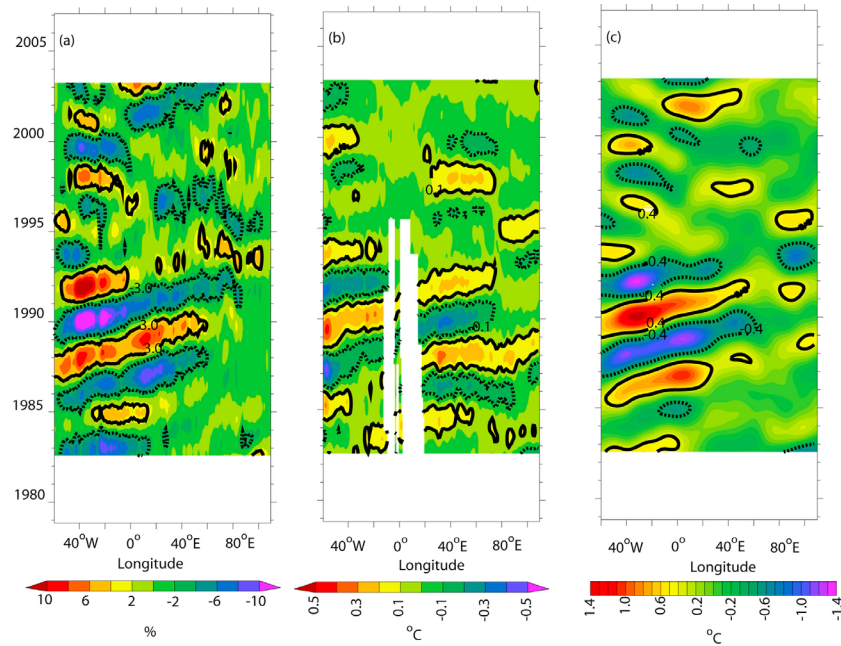


Figure 1. Hovmoller plot of band-pass filtered anomalies with 3–7 year periodicity in the latitudinal band 58°–60°S for: (a) sea-ice concentration (b) SST anomaly and (c) air temperature anomaly. Contours enclose values greater than one standard deviation. Dashed contours represent negative values.

showed that temperature anomaly can be propagated eastward by mean zonal winds if the atmosphere is regarded as barotropic. These studies underline the importance of air-sea coupling and ACC in the propagation of anomalies observed in the Southern Ocean (SO). Though the ACW is closely linked with the ACC, the circumpolar nature of the ACW is uncertain. Fourier harmonics of SST revealed that the eastward propagating part accounted for only 25% of the total signal [Park *et al.*, 2004]. A clear eastward propagation of the ACW was only found during 1985–95 [Connolley, 2003], the time period based on which White and Peterson [1996] first proposed the existence of an ACW.

[4] Though there are studies that show ACW branches northward in the Indian Ocean sector and reach the Indonesian seas and continue its circuit around the globe [see, e.g., Peterson and White, 1998; White and Annis, 2004], the unorganised nature of the ACW propagation in the ice-ocean-atmosphere system of the Indian Ocean sector was evident in a few studies [e.g., White *et al.*, 2004; Gloersen and White, 2001] (see Figures 2b and 2c between points 1–60 of White *et al.* [2004] and Figure 1 of Gloersen and White [2001]). Moreover, complex EOFs of sea-ice edge depicted eastward anomaly propagation in the central Pacific and Weddell Sea, propagating signals were insignificant and inconsistent in the Indian Ocean [Yuan and Martinson, 2000]. We examine this aspect; why the anomaly propagation is disrupted in the ice-ocean-atmosphere system of the Indian Ocean region.

2. Data and Methods

[5] The aim of the study is to investigate the characteristics of ACW in the Indian Ocean sector of Antarctica. We

analysed the Hadley Centre $1 \times 1^\circ$ sea-ice concentration (SIC) and SST [Rayner *et al.*, 2003] for the time period 1978–2006. The SIC and SST data were band-pass filtered using a Lanczos filter with 91 weights to retain a 3–7 year periodicity. The choice of the number of weights was guided by the length of resulting time series and the frequencies filtered. If more weights were used, the length of the time series was reduced without much effect on filtering. For weights less than 91, the resulting time series was longer, but frequencies greater than 4 years persisted. Since the ACC was found to be a major carrier of climate anomalies in the SO [Venegas, 2003; Cai *et al.*, 1999], geostrophic currents referenced to 1000m were computed from a merged temperature-salinity data set provided by the UK Met Office [Ingleby and Huddleston, 2007]. This is a $1 \times 1^\circ$ objectively analysed data set blending all the available temperature-salinity observation including the ARGO floats. Air temperature and atmospheric vertical velocity in Pa/s (omega) from NCEP/NCAR reanalysis [Kalnay *et al.*, 1996] have been used to understand the role of atmospheric feedback on ACW.

3. Results and Discussion

[6] Figure 1a shows the time-longitude diagram of SIC anomaly filtered to retain the 3–7 year periodicity for the region extending from 60°W to 110°E in the latitude band 58°–60°S. At this periodicity SIC anomaly propagates from west to east. Lag sequences of dominant EEOF of mean wind field and SST were found to propagate around the Indian Ocean sector at latitudes lower than 50S [White, 2000]. However in the ice-ocean-atmosphere system propagating signals were clearly discernable only in the region 60°W to 40°E, more so in the northern latitudes with distinct

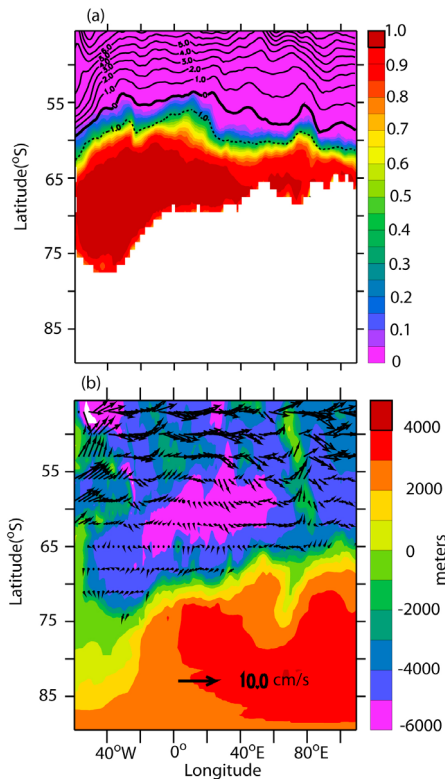


Figure 2. Climatology of (a) sea-ice fraction averaged for the winter (July–Sep) overlaid with SST contours ($^{\circ}\text{C}$), and (b) geostrophic velocity vectors averaged for the winter (July–Sep) overlaid on bottom topography derived from ETOPO60 data.

eastward propagation during the time period 1985 to 1995 (Figure S1 of the auxiliary material).¹ A plot of surface air temperature anomalies showed a similar characteristic, but the propagation became feeble beyond 40°E and maximum amplitudes were observed during 1985–92 (Figure 1c). Therefore, the ACW in the atmosphere and ocean do not exist east of 40°E . In order to address this issue further, climatology of SIC for the winter months (July – Sep.) for the period 1985–91 was constructed (Figure 2a). The winter time sea-ice extent in the Weddell Sea (60°W – 20°E) was almost 5° latitude greater than in the region east of the meander. Geostrophic currents showed a southward velocities in the region 10° – 30°E in the 55° – 65°S belt (Figure 2b). This meandering coincided with a deep bottom topography of about 6000 m (Figure 2b). Thus as the ACC enters the deeper regions it is steered south in order to conserve the potential vorticity. This southward meandering transports warm waters southward and makes the region warmer by about 1°C than to its west (Figure 2a). The mean (standard deviation) of winter time SST in the box 30° – 40°E and 65 to 55S was about 0.06°C (0.2°C) whereas a similar box to the west of the meander within the same latitudinal range between 10°W and 0° had a mean (standard deviation) of -0.9°C (0.15°C). If we restrict the latitudinal range to 60° – 58°S the means (standard deviations) were -0.3°C (0.24°C)

¹Auxiliary materials are available in the HTML. doi:10.1029/2011GL046898.

and -1.4°C (0.16°C) respectively for the eastern and western boxes. Further east (60° – 70°E) between 60° – 58°S the mean (standard deviation) for SST was about -0.12°C (0.2°C). Thus the sea surface has warmed up progressively from west to east in the meandering region.

[7] It may also be noted that Ekman velocities also interact with the propagating ACW anomalies. But the ACW anomalies reach the region of ACC meandering during summer when the Ekman depth is shallowest (Figure S7). Moreover below the Ekman layer the geostrophic flow was southward. The observed sea-ice and SST (Figure 2) seems to be a response to this southward flow that warms up the Indian Ocean region and reduce the ice.

[8] The topographic deflection of the ACC has two repercussions on the ACW propagation. As the ACW propagates along with the ACC the southward deflection advects the anomalies associated with the ACW southward, thus deviating from its normal west – east route. Secondly the warming associated with the southward meandering does not allow sea-ice formation. East of the meander we observed SST close to -0.1° to 0°C . Though the mean and standard deviation of SST were not conducive for ice formation, sea-ice can be found just east of the meander (up to 40°E) in low concentrations. However further east sea-ice was almost absent. For sea-ice formation the water temperature must fall below the freezing point, which is -1.86°C for a salinity of about 33.8 psu. In the present case the SST anomaly propagation associated with ACW only accounts for a maximum of about ± 0.3 – 0.5°C in the region east of the meander (Figure 1b). Thus the maximum negative SST anomaly can be -0.3 to -0.5°C which cannot initiate anomalous SIC. Moreover ice begins to melt as the anomalies interact with warm waters east of the meander and reduce its strength west to east.

[9] However, since the ACW is a coupled ocean-atmosphere phenomenon, its imprints could be found in the ocean if strong air temperature anomalies propagated east of 40°E . But, atmospheric temperature anomalies associated with the ACW also reduced its strength eastward of 40°E (Figure 1c) and surface air temperature showed warming signatures ($\sim 6^{\circ}\text{C}$ warmer than the west) coinciding with the ACC meandering (Figure S2a). A reduction in eastward propagating anomalies may be due to the following factors. First, the meandering of ACC affects the oceanic anomaly propagation in the region east of the meander. This could decouple the ACW as a combined ocean-atmosphere eastward propagating system. However, it is interesting to note that like oceanic anomalies, atmospheric anomalies also reduced their strength after crossing 20° and is barely traceable after 40°E . Thus we infer that processes specific to the region east of 20° lead to the discontinuity in ACW propagation in the Indian Ocean. The southward meandering of the ACC resulted in a west-east SST front, with warm waters to the east and cooler waters to the west. This east-west contrast in SST could generate secondary circulation. Omega values obtained from NCEP/NCAR reanalysis showed conspicuous upward motion (convection) in the 40 – 60°E belt and descending motion to its west (0° – 40°E) (Figure S2b). This circulation is known to partly cancel the horizontal thermal advection by adiabatic temperature changes of rising motion [Holton, 2006]. In order to investigate this we studied three most conspicuous eastward propagating anomalies that began in 1985, 87 and 1989

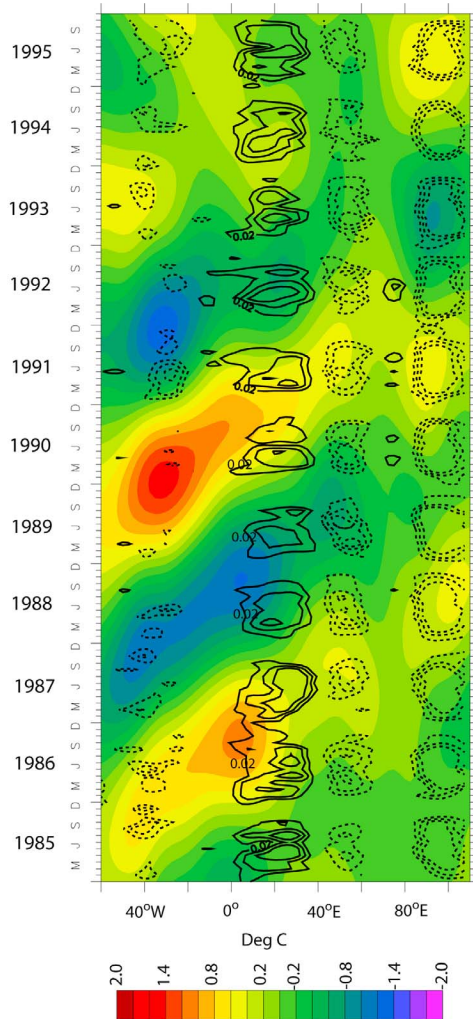


Figure 3. Air temperature anomalies bandpass filtered to retain a 3–7 year periodicity overlaid with vertical velocity in Pa/s. Contour intervals are at 0.01 Pa/s. Vertical velocity contours greater than one standard deviation are shown.

(Figure 3). Of these, 1985 and 1989 were warm anomalies. Warm and cold anomalies could be generated in the Weddell Sea during ENSO years. The mechanisms leading to climate anomalies in the Weddell Sea were explained by Yuan [2004]. Suffice to state here that during a cold/warm ENSO event, the Weddell Sea region becomes warmer/colder. Thus, two warm and cold ACW anomalies were formed. Once generated, these anomalies propagate through the Weddell Sea and reach the Indian Ocean region in about a year where the vertical velocity peaks during March to September each year. Omega values indicated an average of ± 0.02 to 0.04 Pa/s or ± 0.2 to 0.3 cm/s at the surface in the Indian Ocean region. At this velocity air parcels rise/sink to about 5–7 km per month. Whether this slow vertical motion leads to adiabatic temperature changes is doubtful, as the air parcels get enough time to interact with the ambient conditions. Also, had the adiabatic changes been guiding the ACW changes, we would have noticed intensification of warm anomalies in the region 0° – 40° E. Rather, we noticed reduction in ACW strength irrespective of warm/cold

anomalies. As the ACW propagated as a coupled ocean-atmosphere system, a reduction in ACW strength can arise from the decoupling of ocean-atmosphere anomalies by topographic meandering. In the region, between 0° and 40° E the eastward velocity was nearly zero (Figure S3). This not only slowed down the eastward oceanic ACW but advected it southward as well. This sudden change in ocean surface velocities decelerated the west-east propagation of oceanic anomalies and weakened the ACW. Weakened anomalies propagated further eastward and reached the region 40° – 60° E, where the upward velocities reached a maximum. The slope of the ACW anomalies revealed an average speed of ~ 7 cm/s, or ~ 180 km/month. Thus, as the ACW travelled 180 km horizontally, present vertical velocities could advect the anomalies vertically to about 5–7 km in the region 40° – 60° E, where surface oceanic currents were southeasterly. An estimation of the horizontal ($u\partial T/\partial x$, $v\partial T/\partial y$) and vertical advection ($w\partial T/\partial z$) terms in the temperature equation for the atmosphere showed that in the Indian Ocean region, the vertical advection has a magnitude similar to that of horizontal advection. Moreover in the region 40° – 60° E, meridional and vertical advective terms dominated the zonal advective term that is close to zero (Figure S4). This supports the termination of zonal propagation of ACW in the Indian Ocean region. Thus, unlike the original ACW in which both oceanic and atmospheric anomaly propagate eastward, in the Indian Ocean region atmospheric/oceanic ACW anomalies have a tendency to move vertically up/southward. This inhibited the eastward propagation of ACW as a coupled ocean-atmosphere system in the Indian Ocean. Thus, as the ACW enters the Indian Ocean sector it is driven southward by the ACC due to topographic effect, which decouples the atmospheric and oceanic anomalies, the atmospheric anomalies may propagate further in to the region where zonal advection is zero, hence the anomalies tend to advect meridionally and upward. This is schematically illustrated in Figure 4. However it has been shown in literature that ACW propagates in the Pacific and the Ross Sea sectors. In order to examine this we present the advective terms (Figure S5) and the zonal geostrophic velocities (Figure S6) along the same latitudinal band across the globe. Two inferences can be drawn from this analysis: First, the zonal geostrophic velocity in the region between 0° and 50° E was found to be less than zero, so no eastward

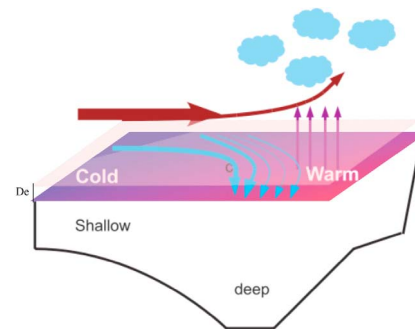


Figure 4. Schematics of ACW propagation in the Indian Ocean sector of Antarctica. The topographic meandering decoupled the atmospheric and oceanic anomalies by southward deflection of ACC and upward motion developed in response to the east-west SST front generated by the topographic meandering. D_E is the Ekman depth.

propagation takes place. Second, vertical velocity in the atmosphere is maximum in the Indian Ocean region. The reasons for low vertical velocities in the atmosphere away from the Indian Ocean region are not well understood. But this confirms the ACW propagation in the Pacific (120–180°E) and Ross Sea sectors (180–135°W) and its termination in the Indian Ocean region.

4. Conclusions

[10] The study investigates the characteristics of propagation of the ACW in the ice-ocean-atmosphere system of the SO. Our study confirms that the ACW signal does not propagate east of 40°E. Nevertheless, east of 40°E sea surface is found to be about 1°C warmer than to its west. We infer that this enhanced SST is due to the topographic meandering of the ACC, which transports warm water southward and reduces sea-ice extent in the region between 20° and 80°E. The anomalies associated with the ACW are unable to negotiate the topographic meandering primarily due to two reasons. First, as the ACC is steered south, eastward propagating anomalies are also advected southward, deviating from its original east-west path. Furthermore, a reduction in amplitude of positive SIC is observed as it interacts with the warmer waters to the east. Similar to oceanic ACW anomalies, atmospheric anomalies are also distinct west of 0°. Deceleration of oceanic ACW anomalies by topographic meandering of the ACC results in a weakening of atmospheric anomalies as well by the interaction with atmospheric vertical velocities. This totally decouples the ACW anomalies in the Indian Ocean sector and makes further eastward propagation impossible. Away from the Indian Ocean region vertical advection is found to be lower and marked by positive zonal velocity of the ACC. This promotes the ACW propagation in the Pacific sector and the Weddell Sea.

[11] **Acknowledgments.** The authors thank Director NCAOR for his keen interest and encouragement for this study. This work was carried out under the project “Delineation of sea ice Boundary from India Bay to Larsemann Hills, Antarctica Using High Resolution Satellite Imagery” and a fellowship awarded by Scientific Committee on Antarctic Research (SCAR). Yuan is supported by US NSF OPP grant ANT07-39509. NCEP reanalysis data was provided by the NOAA/OAR/ESRL PSD, Boulder, Colorado, USA, from their web site <http://www.esrl.noaa.gov/psd/>. Hydrographic data was downloaded from Met Office Hadley Centre website http://hadobs.metoffice.com/en3/data/EN3_v2a/download_EN3_v2a.html. SST and ice data were obtained from Met Office Hadley Centre web site <http://hadobs.metoffice.com/hadisst/data/download.html>. M. Nuncio thanks Dina and Ramola Antao for carefully going through the manuscript for grammar and style. This is NCAOR contribution 07/2011 and Lamont contribution 7463.

[12] The Editor thanks two anonymous reviewers for their assistance in evaluating this paper.

References

- Cai, W., and P. G. Baines (2001), Forcing of the Antarctic Circumpolar Wave by El Niño-Southern Oscillation teleconnections, *J. Geophys. Res.*, *106*, 9019–9038, doi:10.1029/2000JC000590.
- Cai, W., P. G. Baines, and H. B. Gordon (1999), Southern mid to high-latitude variability, a zonal wavenumber-3 pattern, and the Antarctic Circumpolar Wave in the CSIRO coupled model, *J. Clim.*, *12*, 3087–3104, doi:10.1175/1520-0442(1999)012<3087:SMTHLV>2.0.CO;2.
- Christoph, M., T. P. Barnett, and E. Roeckner (1998), The Antarctic Circumpolar Wave in a coupled ocean-atmosphere GCM, *J. Clim.*, *11*, 1659–1672, doi:10.1175/1520-0442(1998)011<1659:TACWIA>2.0.CO;2.
- Comiso, J. C. (2000), Variability and trends in Antarctic surface temperatures from *in situ* and satellite infrared measurements, *J. Clim.*, *13*, 1674–1696, doi:10.1175/1520-0442(2000)013<1674:VATIAS>2.0.CO;2.
- Connolley, W. M. (2003), Long term variation of the Antarctic Circumpolar Wave, *J. Geophys. Res.*, *108*(C4), 8076, doi:10.1029/2000JC000380.
- Fischer, H., F. Traufetter, H. Oerter, R. Weller, and H. Miller (2004), Prevalence of the Antarctic Circumpolar Wave over the last two millennia recorded in Dronning Maud Land ice, *Geophys. Res. Lett.*, *31*, L08202, doi:10.1029/2003GL019186.
- Gloersen, P., and W. White (2001), Re-establishing the circumpolar wave in the sea-ice in the Antarctica from one winter to next, *J. Geophys. Res.*, *106*, 4391–4395, doi:10.1029/2000JC000230.
- Haarsma, R. J., F. M. Selten, and J. D. Opsteegh (2000), On the Mechanism of the Antarctic Circumpolar Wave, *J. Clim.*, *13*, 1461–1480, doi:10.1175/1520-0442(2000)013<1461:OTMOTA>2.0.CO;2.
- Holton, J. R. (2006), *An Introduction to Dynamical Meteorology*, Elsevier, Amsterdam.
- Ingleby, B., and M. Huddleston (2007), Quality control of ocean temperature and salinity profiles, historical and real time data, *J. Mar. Syst.*, *65*(1–4), 158–175, doi:10.1016/j.jmarsys.2005.11.019.
- Jacobs, G. A., and J. L. Mitchell (1996), Ocean circulation variations associated with the Antarctic Circumpolar Wave, *Geophys. Res. Lett.*, *23*, 2947–2950, doi:10.1029/96GL02492.
- Kalnay, E., et al. (1996), The NCEP/NCAR 40-year reanalysis project, *Bull. Am. Meteorol. Soc.*, *77*, 437–471, doi:10.1175/1520-0477(1996)077<0437:TNYRPP>2.0.CO;2.
- Park, Y.-H., F. Roquet, and F. Vivier (2004), Quasi-stationary ENSO wave signals versus the Antarctic Circumpolar Wave scenario, *Geophys. Res. Lett.*, *31*, L09315, doi:10.1029/2004GL019806.
- Qiu, B., and F. F. Jin (1997), Antarctic circumpolar waves: An indication of ocean-atmosphere coupling in the extra tropics, *Geophys. Res. Lett.*, *24*, 2585–2588.
- Rayner, N. A., D. E. Parker, E. B. Horton, C. K. Folland, L. V. Alexander, D. P. Rowell, E. C. Kent, and A. Kaplan (2003), Global analyses of sea surface temperature, sea ice, and night marine air temperature since the late nineteenth century, *J. Geophys. Res.*, *108*(D14), 4407, doi:10.1029/2002JD002670.
- Talley, L. D. (1999), Simple coupled midlatitude climate models, *J. Phys. Oceanogr.*, *29*, 2016–2037, doi:10.1175/1520-0485(1999)029<2016:SCMCM>2.0.CO;2.
- Venegas, S. A. (2003), The Antarctic Circumpolar Wave: A combination of two signals?, *J. Clim.*, *16*, 2509–2525, doi:10.1175/1520-0442(2003)016<2509:TACWAC>2.0.CO;2.
- White, W. B. (2000), Influence of Antarctic Circumpolar Wave on Australian precipitation, *J. Clim.*, *13*, 2125–2141, doi:10.1175/1520-0442(2000)013<2125:IOTACW>2.0.CO;2.
- White, W. B., and J. Annis (2004), Influence of Antarctic Circumpolar Wave on El Niño and its multi decadal changes from 1950 to 2001, *J. Geophys. Res.*, *109*, C06019, doi:10.1029/2002JC001666.
- White, W. B., and R. G. Peterson (1996), An Antarctic circumpolar wave in surface pressure, wind and sea ice extent, *Nature*, *380*, 699–702, doi:10.1038/380699a0.
- White, W. B., S. C. Chen, and R. G. Peterson (1998), The Antarctic Circumpolar Wave: A beta effect in ocean-atmosphere coupling over Southern Hemisphere, *J. Phys. Oceanogr.*, *28*, 2345–2361, doi:10.1175/1520-0485(1998)028<2345:TACWAB>2.0.CO;2.
- White, W. B., S. C. Chen, R. J. Allan, and R. C. Stone (2002), Positive feedbacks between the Antarctic Circumpolar Wave and the global El Niño-Southern Oscillation Wave, *J. Geophys. Res.*, *107*(C10), 3165, doi:10.1029/2000JC000581.
- White, W. B., P. Gloersen, and I. Simmonds (2004), Tropospheric response of Antarctic Circumpolar Wave along the sea-ice edge around Antarctica, *J. Clim.*, *17*, 2765–2779, doi:10.1175/1520-0442(2004)017<2765:TRITAC>2.0.CO;2.
- Yuan, X. (2004), ENSO-related impacts on Antarctic sea ice: Synthesis of phenomenon and mechanisms, *Antarct. Sci.*, *16*(4), 415–425, doi:10.1017/S0954102004002238.
- Yuan, X., and D. G. Martinson (2000), Antarctic sea-ice extent variability and its global connectivity, *J. Clim.*, *13*, 1697–1717, doi:10.1175/1520-0442(2000)013<1697:ASIEVA>2.0.CO;2.

A. J. Luis and M. Nuncio, National Centre for Antarctic and Ocean Research, Headland Sada, Vasco da Gama, Goa 403804, India. (nuncio@ncaor.org)
X. Yuan, Ocean and Climate Physics Laboratory, Lamont Doherty Earth Observatory, 61 Rte. 9W, Palisades, NY 10964, USA.